Structural, optical and electronic characteristics of non-stoichiometric nano cadmium sulfide

Zein K. Heiba
Ain shams University
Mohamed Bakr Mohamed
Taibah University
Noura M. Farag
Ain Shams University
Ali Badawi (adaraghmeh@yahoo.com)
Taif University https://orcid.org/0000-0002-3068-9609

Research Article

Keywords: Non-stoichiometric sulfur, oxygen, structure, optical

Posted Date: February 26th, 2021

DOI: https://doi.org/10.21203/rs.3.rs-246763/v1

Version of Record: A version of this preprint was published at Journal of Materials Science: Materials in Electronics on March 6th, 2021. See the published version at https://doi.org/10.1007/s10854-021-05615-0.

Abstract

Samples of non-stoichiometric nano CdS_{1-x} were synthesized by a simple thermolysis method by lowering the ratio of thiourea relative to cadmium acetate as starting precursors; Cd(Ac):(1-x) thiourea (x = 0.0, 0.03, 0.05 and 0.1). X'pert HighScore Plus program manifested biphasic CdS (cubic and hexagonal) and the Rietveld analysis was utilized to match the structural and microstructure parameters of the formed samples. The possibility of formed $CdS_{1-x}O_x$ alloy due to the sulfur deficiency is also examined using the Rietveld method. A High-resolution transmission electron microscope imaging exhibited nano size particles with homogeneous morphology. Fourier transform infrared spectrometer was utilized to confirm the existence of O_2 in CdS_{1-x} matrix. The bandgap energies for CdS_{1-x} are reduced below the values of energy gaps of CdS and CdO upon increasing the parameter (x) forming a band gap "bowing". The photoluminescence (PL) emitted visible colors depending on the amount of sulfur deficiency and excitation wavelength used. The maximum PL intensity observed in $CdS_{0.9}$ sample, confirmed the presents of oxygen inside the matrix. The influence of oxygen substitution or vacancies of sulfur on the electronic structure and optical features of CdS was also investigated applying density function calculations.

1. Introduction

In the last years, inorganic semiconductor materials such as ZnS, ZnO, CdS, SnS_2, CuS or CdSe [1–6] have been broadly considered due to their uses in the people's daily life. Furthermore, the nanostructures of the semiconductor materials revel an interesting linear absorption, photoluminescence emission and nonlinear characteristics as compared with bulk form [1–6]. Cadmium sulfide (CdS) is a familiar semiconductor photocatalytic material that possesses a wide bandgap ≈ 2.4 eV [3], and it exhibited a rapid generation of photo-induced electron-hole pairs [7]. Unfortunately, CdS has rapid recombination of carriers and photocorrosion which limited its uses in photocatalytic activity [8]. Furthermore, CdS needed high temperatures and expensive inert environments during preparation with traditional methods [9]. Several methods were used to prepare CdS in different size, shape and morphology to enhance its stability and photocatalytic activity under visible light [10]. CdS can crystallize in one or more phases (cubic zinc blend, hexagonal wurtzite, rock-salt phase) [11]. CdS can be found with the hexagonal phase under ambient conditions, while CdS with the cubic phase can exist when the crystallite size reduced. Finally, under applying high pressure, CdS with the rock salt structure can be obtained [12]. It was found that the number of vacancies (V_{cd}), cadmium interstitial (I_{cd}) and stacking faults defects affect the structure transformation of CdS from one phase to another [13]. CdS with mixed hexagonal and cubic phases can be obtained as it has a crystallize size of 4–5 nm, while it is formed either in cubic or hexagonal only when the crystallite size below or above this crystallite size value, respectively [14]. On the other hand, changing the ratio of S to Cd in CdS samples to be non-stoichiometric can transfer the structure of CdS from hexagonal to cubic configuration [15] or produce CdS with two crystal structures (cubic and hexagonal); all these factors affect the physical features of the material [16]. CdS formed as a [illegible] a higher photocatalytic H_2 production than CdS

nanorods with a hexagonal structure with photocatalytic stability over 400 h [17]. Shen et al. varied the Cd to S ration during preparation CdS by the solvothermal method to control the zinc-blende and wurtzite structures inside the formed material to investigate their photocatalyst performance [18]. Vaquero et al. prepared CdS also by solvothermal method but they changed the annealing temperature and water/thiourea ratio during the preparation of CdS sample, they found all formed sampled exhibited a hexagonal structure only [19]. Pandya et al. found the energy gap of CdS thin film; regardless of the Cd amount with respect to the S amount [20]. On the other hand, CdO is an n-type semiconductor with a direct optical bandgap 2.2–2.5 eV and high transparency over a wide spectral range and higher electron mobility compared with CdS [21]. It was found the photocatalytic effect of CdO-CdS to produce hydrogen from water composites is better than CdO or CdS nanoparticles alone [22]. Very few reports have been published on the synthesis and characteristics of Cd(S/O) films [23]. Oxygen incorporated in nanocrystalline CdS films to form $CdS_{1-x}O_x$ alloy improved solar cell performance [23]. Moreover, the optical bandgap of Cd(S/O) films reduced from 2.34 eV for CdS to 2.26 eV according to the CdO amount in the film [24]. Non-stoichiometric CdS can adjust the band gap with new optical properties. The current study is aimed to explore the effect of changing the Cd:S ratio in the starting precursors on the characteristics of the formed CdS. As mentioned above, there are a lot of different procedures were used to produce the nano materials, among of them the thermolysis technique which does not need a solvent during the reaction and produces a large mass scale amount. Non-stoichiometric CdS nano materials were formed applying a thermolysis process; cadmium acetate: (1-x) thiourea, x = 0.0, 0.03, 0.05 and 0.1. X-ray diffraction phase investigation was performed to determine the phases developed in the CdS_{1-x} samples and to study the possibility of oxygen incorporate in the formed system. The structural, microstructural, and optical properties of the formed samples have been investigated applying X-ray diffraction, high-resolution transmission electron microscope (HRTEM), Fourier transform infrared spectrometer, photoluminescence, and UV–Vis devices. DFT calculation was applied to study the electronic and optical features of CdS, in the case of existence of some sulfur vacancy in CdS matrix ($CdS_{0.9}$) or substituted of some sulfur by oxygen in CdS matrix ($CdS_{0.9}O_{0.1}$).

2. Methods And Materials

Non-stoichiometric CdS nano materials were synthesized applied a thermolysis process, where the thiourea amount was reduced as compared with the amount of cadmium acetate in the beginning of synthesis. Different non-stoichiometric parameter (x) was applied: cadmium acetate:(1-x) thiourea, x = 0.0, 0.03, 0.05 and 0.1, for simplicity let`s called the formed compounds CdS_{1-x} (x = 0.0, 0.03, 0.05 and 0.1). The required amount of cadmium acetate dihydrate Cd $(CH_3COO)_2.2H_2O$, 98%) and thiourea [$SC(NH_2)_2$, 99.98%,] for each compound were ground, then heated in an electric furnace (200 ºC for 3h), Fig. 1. MAUD program [25] depended on the Rietveld profile technique [26] was carried out to examine the crystal structure and microstructure of the formed CdS_{1-x} system. The techniques X-ray diffraction (X'pert MPD, Philips with Cu-K_α source), high resolution transmission electron microscope (HRTEM), Fourier transform infrared (FTIR, Bruker Tensor 27 FTIR spectrometer), UV–Vis (Shimadzu UV-3101PC ectrophotometer (RF-1501 SHIMADZU, Ltd))

were utilized for careful investigations all samples. Different electronic structure's parameters were obtained applying Cambridge sequential total energy package (CASTEP) code [27] relies on first principle calculation. The supercell of CdS with cubic structure, 2·1·1-unit cell dimension, ultra-soft pseudopotentials, GGA-PBE conditions and energy cutoff (380 eV) [28, 29], more details can be found in [16]. The $4d^{10}5s^2$ and $3s^23p^4$, electrons relevant to Cd and S atoms were employed for the pseudopotential arrangements, respectively. For comparing the DFT calculations for some sulfur vacancy in CdS ($CdS_{0.9}$) with those for some sulfur substituted by oxygen in CdS ($CdS_{0.9}O_{0.1}$), the previous criteria were applied.

3. Results And Discussions

3.1. XRD structural investigation

X-ray diffraction patterns have been measured, Fig. 2a, with high quality (small 2θ-step and linear detector) for accurate structural and microstructural analysis. Applying the program X'pert HighScore plus, all samples CdS_{1-x} ($0 \leq x \leq 0.1$) manifested pure CdS structure. Also, two CdS phases are detected in all samples; cubic $F\bar{4}3m$ and hexagonal P 6_3 m c with the cubic phase a little bit dominant, Table 1. Structural analysis is carried out applying Rietveld method; Fig. 2b displays the obtained pattern fitting for x = 0.03 as example. The crystallite sizes of the two phases are quite similar with an average value around 5 nm. Figure 2c, d shows the HTEM images with different magnifications. Homogenous morphology and a uniform size (almost no size distribution) can be noticed with a very small size resembling quantum dots (around 5 nm), but the particles are highly agglomerated. The inset image of Fig. 2d illustrates a set atom planes with high degree of dislocations arising from vacant sites due to sulfur deficiency and/or oxygen incorporation into the CdS lattice. Rietveld analysis emphasized that O atoms are introduced into the CdS_{1-x} lattice to recompense the sulfur deficiency, producing an alloy $CdS_{1-x}O_x$. Better fitting of diffraction pattern demands the incorporation of O in vacant sites of sulfur. Furthermore, during Rietveld analysis, O ions are found to compensate S atoms substitutionally at the crystallographic site of sulfur; trails to reside O atoms in the interstitial voids in CdS lattice yield poor pattern fitting with bad reliability factors. Oxygen diffusion into ZnSe, CdSe, and CdS semiconductors upon air annealing has been detected in x-ray quantitative phase's study [30]. Similar results obtained for annealed ZnTe; O atoms were diffused into the lattice before the semiconductor was oxidized [31]. The refined structural parameters and the phases percentage obtained for CdS_{1-x} ($0 \leq x \leq 0.1$) applying Rietveld analysis are given in Table 1. The lattice parameters for both cubic and hexagonal phases are obviously decreased upon increasing (x). The decrease in lattice parameters may be attributed to the incorporation of O atoms to compensate for S atoms and/or the formation of some vacancies in the lattice. As in Table 1, the z-coordinate of the S/O atoms z(S/O) in the hexagonal phase is also decreased with the parameter (x), resulting in increasing the bond length distortion index.

Table 1
Lattice parameter, a (Å), average crystallite size nm, and phase percentage for CdS_{1-x} samples.

	CdS							
x	Cubic $F\bar{4}3m$			Hexa P 6_3 m c				
	a	size	%	*a*	*c*	size	z(S/O)	%
0.0	5.875(4)	6	55	4.131 (3)	6.787(4)	5	0.3781	45
0.03	5.837	5	55	4.125	6.780	5	0.3741	45
0.05	5.828	4	57	4.120	6.778	5	0.3698	43
0.10	5.831	5	54	4.123	6.775	6	0.3679	46

3.2. Infrared absorption spectroscopy study

The FTIR spectra measured for the non-stoichiometric nano CdS_{1-x} (x = 0.0, 0.03, 0.05 and 0.1) are depicted in Fig. 3. All the spectra exhibit peaks in the low wavelength region 445, 543, 580, 612, and 684 cm^{-1} representing the stretching mode of Cd–S bond [32]. The inset figure manifests the shift of these bands with the parameter non-stoichiometry (x) indicating the insertion of O_2 into the CdS lattice replacing the S atoms. The observed bands at 1400–1540 cm^{-1} can be ascribed to the carboxyl group [33] and the band at 1620 cm^{-1} represents C = O stretching modes and/or O − H bending vibration; both happened due to the absorbed atmospheric CO_2 and humidity on the surface of the nanocrystals [33]. The active vibrations related to the O − H are observed in the range from 3300–3500 cm^{-1} for the stretching mode [34]. The weak band around 2000–2250 cm^{-1} is attributed to C = C stretching vibration mode [35].

3.3. UV absorption analysis

Figure 4a reveals the UV absorption as function of wavelength (300–800 nm) for the non-stoichiometric CdS_{1-x} (x = 0.0, 0.03, 0.05 and 0.1) samples. A broad absorption band is obtained for all samples and its position is changed with the non-stoichiometry parameter (x). Rietveld refinement indicated that oxygen atoms are introduced into the CdS_{1-x} matrix to recompense the sulfur deficiency and producing an alloy $CdS_{1-x}O_x$. Both CdS and CdO are direct bandgap semiconductors, accordingly, $CdS_{1-x}O_x$ is assumed also a direct bandgap semiconductor. The optical bandgap (E_g) of $CdS_{1-x}O_x$ samples was estimated applying the Tauc plot, Fig. 4, using the following relation for the direct transition:

$$\alpha h\nu = C(h\nu - E_g)^{0.5}$$

where C is a constant, hv is the incident photon energy and α is the absorption coefficient, respectively.

Although the optical bandgap of the $CdS_{1-x}O_x$ was expected have a value intermediate to that of the CdS (~ 2.4 eV) and CdO (~ 3.1 eV) [36], the obtained bandgap energies are reduced below these values upon increasing the parameter (x) forming a band gap "bowing", Fig. 4b. Such a bandgap bowing was detected for $ZnS_{1-x}O_x$ [37] and was interpreted by applying first-principles calculations [38]. For small contents of oxygen (x), the energy value of the conduction band (CBM) minimum is reduced whereas the valence band energy is nearly not changed, which caused a decrease in the optical bandgap energy. Furthermore, this shift in CBM is due to the hybridization between the oxygen 3*s* state and ZnS conduction-band states [39]. As the concentration of oxygen (x) increased, the conduction band staying nearly unchanged and the valance band maximum (VBM) energy is reduced; therefore, the bandgap energy enlarged once more [38]. For the present system $CdS_{1-x}O_x$, the same interpretation may be applied; hybridization between the oxygen 3*s* state and the conduction-band states of CdS can occur leading to a narrowing in the bandgap for low oxygen incorporation, then the bandgap energy increases again for high values of (x).

3.4. Photoluminescence analysis

Figure 5 shows the Gaussian fitting of the broad photoluminescence (PL) spectra of nano CdS_{1-x} system under 350 nm excitation at room temperature. The PL intensity of the sample varied irregular depended on the x value, and it reached it maximum value in $CdS_{0.9}$ sample. Furthermore, samples with x = 0, 0.03, 0.05 and 0.1 can be deconvoluted using Gaussian function in ORIGIN PRO 9.0 software, into (violet, blue, green), (violet, blue, two greens, orange), (blue, two greens, orange), and (violet, two blues) sub-emissions colors, respectively, Table 2. The corresponding goodness of fitting parameter (R-square) values are written in each figure. On the other hand, as Cd_{1-x} system exited with 375 nm, Fig. 6, Gaussian fitting revealed (blue, two greens), (blue, green, orange), (violet, blue) and (two blues, green, orange) colors for x = 0, 0.03, 0.05 and 0.1, samples, respectively, Table 2. The proposed schematic of various possible transitions for all samples are revealed in Figs. 5 and 6. It is known that vacancies and interstitial of sulfur or cadmium (V_S, V_{Cd}, I_S, I_{Cd}) atoms formed during the preparation of nano CdS are the most adsorbed types of defects existed on its surface [40]. When sulfur ions is less than cadmium ions, sulfur vacancies and/ or interstitial are formed [40] and therefore, the PL emission may be due to the surface electron traps by sulfur vacancy or cadmium atoms adsorbed on the surface [41]. The recombination of this trapped electron by sulfur vacancy with a hole in the valence band caused a broad band PL emission with a red shift [42]. On the other hand, when sulfur ions concentration is larger than cadmium ions concentration, interstitial sulfur or cadmium vacancies are formed [43]. These defects can work as hole traps located above the valence band, caused also a broad band PL emission and red shift [43]. CdS nanoparticles obtained by the co-precipitation method revealed a green emission [44, 45]. Mishra et al. found that CdS quantum dot emitted green, yellow, orange and red colors [46]. CdS quantum dots prepared by a post-synthesis modification with aqueous solutions of NaOH emitted violet-blue colors [47]. CdS nanoparticles obtained by the chemical precipitation method utilizing polyvinylpyrrolidone as a capping agent revealed blue and green colors [48]. CdS prepared by hydrothermal technique exhibited blue and green emissions [49]. The emitted colors of CdS_{1-x} can be described as follows (i) violet-blue band is ascribed to the band- edge emission [47], (ii) the green color can be accredited to transitions from

the donor sulfur vacancy levels to the valance band and (iii) the orange emission color could be due to the recombination of defect complexes (I_{cd}-V_{cd})[50]. The bandgap energy of bulk CdS and CdO are very near to each other (2.4 and 2.3 eV) [51]. Thus, the emission characteristics of both are comparable and peak maxima roughly have a similar position. CdO-CdS synthesized in ethylene glycol water mixture emitted green and yellow colors [51, 52]. It also observed the PL intensity of CdO-CdS samples is larger than CdO or CdS nanoparticles [51]. This improvement in intensity may due to the fine mixing of both CdS and CdO phases in the sample. This also indicated the enhancement in the light absorption features and emphasized the high surface area of the samples due to their quantum dots sizes as compared with CdS or CdO alone [51].

3.5. Electronic analysis

CdS with cubic structure (space group F-43m) was used in this calculation as an initial model. The lattice parameter (a) and atoms positions were obtained from X-ray refinement part. The lattice parameter was optimized after geometry relaxation for CdS, $CdS_{0.9}O_{0.1}$ and $CdS_{0.9}$ samples. The obtained lattice parameter after relaxation was 5.9133, 5.8412 and 5.7628 Å for CdS, $CdS_{0.9}O_{0.1}$ and $CdS_{0.9}$ samples, respectively. As noticed from the XRD part the lattice parameter (Table 1) reduced as the sulfur content in the sample reduced. This result indicated that after sulfur amount decreased in CdS sample, may be some vacancies and oxygen are present together in the matrix and this result is consistent with the lattice parameter obtained from DFT calculation. Figure 7 shows the electronic band structure at high-symmetry points of the Brillouin zone for cubic CdS, $CdS_{0.9}O_{0.1}$ and $CdS_{0.9}$ samples. The Fermi energy level is located at zero of the band structure. The figure demonstrated that both the maximum of the valence band (VBM) and the minimum of the conduction band (CBM) for CdS and $CdS_{0.9}O_{0.1}$ samples are situated on the G–path in the Brillouin zone and they have direct bandgaps of 1.142 and 0.809 eV, respectively, which are lower than the experiment values, 2.23 and 2.09 eV for CdS and $CdS_{0.9}O_{0.1}$ samples obtained from UV analysis, Fig. 4. The values of band gap energies obtained from DFT calculations are underestimated, which always happens in DFT analysis due to the recognized limitation of calculating accurate energy band features [53]. In the case of sulfur vacancies sample, $CdS_{0.9}$, the direct bandgap enhanced to 1.823 eV as compared with the energy gap of CdS but it is smaller than the value extracted from UV analysis (2.09 eV). In the case of $CdS_{0.9}O_{0.1}$, the energy gap decreased as compared with CdS. In the case under the study, the energy gap got from UV analysis for $CdS_{0.9}$ sample is less than the energy gap of CdS sample, which indicated that as the content of sulfur reduced in the CdS_{1-x} samples, most of the empty places are occupied by oxygen as indicated from DFT analysis.

The total and partial density of state (PDOS) for Cd, and S atoms are revealed in Fig. 8 for CdS, $CdS_{0.9}O_{0.1}$ and $CdS_{0.9}$ samples. The dotted vertical line in all figures stands for the Fermi level. The total density of state (TDOS) of CdS, $CdS_{0.9}O_{0.1}$ and $CdS_{0.9}$ samples revealed that the valence band has three regions. The maximum of the valence band (VBM) is principally constructed from the *p*-states of both sulfur and cadmium atoms near the Fermi-level in all samples, as revealed in the partial density of state (PDOS). The S-*p* and Cd-*d* states created the middle region of the valence band (VB). The S-*s* and Cd-*s,p,d*

states built the lower part of VB. In the case of $CdS_{0.9}O_{0.1}$ and $CdS_{0.9}$ samples the intensity of VBM is lower than of CdS sample. Additionally, the conduction band (CB) is mostly formed from Cd-*s,p* atom and a small part shared from the S-*p* atom. Furthermore, the density of the state of CB exhibited more split and shifted to low energy part in $CdS_{0.9}O_{0.1}$ sample but it merged and shifted to high energy part in $CdS_{0.9}$ sample.

In order to obtain further features of these three samples, several optical parameters such as optical absorption, dielectric function $\varepsilon(\omega)$ (real part, $\varepsilon_r(\omega)$, and imaginary part, $\varepsilon_i(\omega)$), refractive (n), extinction (k) indices and optical conductivity have been calculated using Kramers-Kronig equations [54]. Figure 9 shows the variation of absorption spectra of CdS, $CdS_{0.9}O_{0.1}$ and $CdS_{0.9}$ samples with photon energy. Absorption spectrum may come out as a consequence of electrons excitations from the valence to conduction band [55]. Furthermore, the exciton peak (Absorption maxima) of $CdS_{0.9}O_{0.1}$ and $CdS_{0.9}$ samples are shifted slightly to higher energy (blue shift) as compared with CdS sample, which could be owing to quantum confinement effects [55]. The absorption spectra revealed also that the samples exhibited a high absorption in UV range and low absorption in visible and near IR regions. Figure 10 reveals the variation of refractive index, extinction coefficient, dielectric constant and optical conductivity in energy range 0-7.7eV for CdS, $CdS_{0.9}O_{0.1}$ and $CdS_{0.9}$ samples. Figure 10a shows that the refractive index (n) maxim values are 2.58, 2.46, 3.12 are which achieved at 3.39, 1.26, 1.63 eV for CdS, $CdS_{0.9}O_{0.1}$ and $CdS_{0.9}$ samples, respectively. In addition, the static refractive index for pure CdS, $CdS_{0.9}O_{0.1}$ and $CdS_{0.9}$ samples are 2.23, 2.28 and 2.68, respectively. The obtained n value for CdS sample is slightly lower than the experimental value (2.38), obtained at 1.96 eV [55]. Generally, the changes in refractive index values with photon energy may be due to the interaction of light with different atoms, defects, grain boundaries and density of the medium inside the unit cell [55]. Figure 10b reveals the dielectric constant for all samples, where the dielectric behavior of $CdS_{0.9}$ sample is slightly changed as compared with CdS sample. Furthermore, at photon high energy value, the dielectric of both CdS and $CdS_{0.9}O_{0.1}$ samples is higher than $CdS_{0.9}$ sample. In general, the behavior of an increase or decrease in dielectric constant is related to the enhancement or reduction in absorption coefficient and states density [56]. Figure 10c demonstrates the increase in the extinction coefficient (k) value with raise the photon energy. The extinction coefficient represented the absorption of energy at the surface of material [57], as revealed from the figure that the absorption of energy at the surface of $CdS_{0.9}$ sample is higher than other two samples in energy range (2–5 eV), which may be due to the defect exists in this sample due to the decrease of the sulfur amount. The large value of the extinction coefficient of $CdS_{0.9}$ sample allows it to be used in several light harvesting technologies such as photovoltaics and thermo-spectronic based biomedical applications [57]. Figure 10d shows that the optical conductivity maxima of CdS, $CdS_{0.9}O_{0.1}$ and $CdS_{0.9}$ samples are located at 6, 6.2 and 5.2 eV, respectively. After those maximum, optical conductivity decreased with energy. The optical conductivity peaks emerged in UV range and they caused by interband transitions [55]. Furthermore, the optical conductivity for $CdS_{0.9}$ sample is lower than other samples due to the presence of defects result from the decrease of the amount of sulfur in the matrix.

4. Conclusion

X'pert HighScore Plus program manifested that all CdS_{1-x} ($0 \leq x \leq 0.1$) samples have biphasic CdS structures (cubic $F\bar{4}3m$ and hexagonal P 6_3 m c). The cubic phase is a little bit dominant over the hexagonal phase. The crystallite sizes of the two phases are around 5 nm. Rietveld refinement confirmed the presence of O atoms in CdS_{1-x} lattice to recompense the sulfur deficiency producing $CdS_{1-x}O_x$ alloy. The lattice parameters for both cubic and hexagonal phases are decreased upon increasing (x) due to the insertion of oxygen atoms to compensate for S atoms and/or the formation of some vacancies in the lattice. FTIR measurements confirmed the presence of Cd–S stretching mode with a shift in IR bands with the non-stoichiometry parameter (x) indicated the inclusion of O_2 into the CdS lattice. The non-stoichiometric CdS_{1-x} samples have direct bandgap energy less than of CdS and CdO; it changed with (x) forming a band gap bowing due to the change of relative position of the conduction and valance bands. The PL intensity of the samples varied irregular depended on the x value, and it reached its maximum value in $CdS_{0.9}$ sample. CdS_{1-x} samples with x = 0, 0.03, 0.05 and 0.1 revealed (violet, blue, green), (violet, blue, green, orange), (blue, green, orange), and (violet, blue) sub-emissions colors under 325 nm excitation wavelength, respectively. Under 375 nm excitation wavelength, they revealed (blue, green), (blue, green, orange), (violet, blue) and (blue, green, orange) colors, respectively. DFT confirmed that $CdS_{0.9}$ and $CdS_{0.9}O_{0.1}$ have a direct bandgap such as CdS sample. The energy gap of $CdS_{0.9}$ is larger than CdS while $CdS_{0.9}O_{0.1}$ is larger than CdS. DFT calculation confirmed the occupied that empty places (sulfur deficiency) by oxygen. The absorption spectra revealed also that the samples exhibited a high absorption in UV range and low absorption in visible and near IR regions. The refractive index, extinction coefficient, dielectric constant and optical conductivity of $CdS_{0.9}$ and $CdS_{0.9}O_{0.1}$ are different from CdS due to the defects in the matrix. The obtained properties nominated CdS_{1-x} to be used in different optical and sensor applications.

Declarations

Acknowledgement

The Authors thank the support of Taif University Researchers Supporting Project number (TURSP-2020/12), Taif University, Taif, Saudi Arabia.

References

[1] N.Ojha, A.Bajpai, S.Kumar, Journal of Colloid and Interface Science, 585(2021)764.

[2] Y-Q. Wu, Y-S. Zhao, W-J. Meng, Y. Xie, J. Zhang, C-J. He, D-L. Zhao, Applied Surface Science, 539 (2021) 148283.

[3] R. Zeinodin, F. Jamali-Sheini, M. Cheraghizad, Materials Science in Semiconductor Processing, 123(2021)105501.

[4] M. A.R. Alaani, P.Koirala, P. Pradhan, A. B.Phillips, N. J.Podraza, M. J.Heben, R.W.Collins, Solar Energy Materials and Solar Cells, 221(2021) 110907.

[5] J. J. Santaella, K. Critchley, S. Rodríguez-Bolívar, F. M. Gómez-Campos, Nanotechnology, 32(2021) 105204.

[6] R. P.Patila, M. A.Mahadika, W-S.Chae, S. H.Choi, J. S. Jang, Applied Surface Science, 539 (2021) 148267.

[7] S.Y. Ryu, J. Choi, W. Balcerski, T.K. Lee, H.M. R, Ind. Eng. Chem. Res. 46 (2007) 7476.

[8] P.Y. Kuang, P.X. Zheng, Z.Q. Liu, J.L. Lei, H. Wu, N. Li, T.Y. Ma, Small 12 (2016) 6735.

[9] D.B. Bharti, Avinash V. Bharati, Atul V. Wankhade, Luminescence. 33(8)(2018)1445.

[10] P. Zhang, Y. Liu, B.Z. Tian, Y.S. Luo, J.L. Zhang, Catal. Today 281 (2017) 181.

[11]ZK Heiba, MB Mohamed, NG Imam, Journal of alloys and compounds 618 (2015) 280.

[12] A.H. Mueller, M.A. Petruska, M. Achermann, D. Werder, E. Akhadov, D. Koleske, M. Hoffbauer, V.I. Klimov, Nano Lett. 5 (6) (2005) 1039.

[13] R.L. Morales, O.Z. Angel, G.T. Delgado, Appl. Surf. Sci. 175e176 (2001) 562.

[14] R. Banerjee, R. Jayakrishnan, P. Ayyub, J. Phys. Condens. Matter 12 (50) (2000) 10647.

[15] ZK Heiba, MB Mohamed, M Abdellatief, AA Albassam, Applied Physics A 126 (7) (2020)1.

[16] ZK Heiba, MB Mohamed, NY Mostafa, Applied Physics A 125 (2) (2019)132.

[17] K. Li, M. Han, R. Chen, S-L. Li, S-L. Xie, C. Mao, X. Bu, X-L. Cao, L-Z. Dong, P. Feng, Y-Q. Lan, Adv. Mater. 28 (2016) 8906.

[18] Q. Shen, J. Xue, A. Mi, H. Jia, X. Liu, B. Xu, SC Adv.3(2013)20930.

[19] F. Vaquero, J. L. G. Fierro, R. M. N. Yerga, Molecules 21 (2016)401.

[20] S. Pandya, K. Rava, J Mater Sci: Mater Electron, 28, (2017) 18031

[21] R. Ferro, JA RodriAguez, O Vigil, A Morales-Acevedo, G. Contreras-Puente. Phys Status Solidi 177 (2000)477.

[22] S V. Kahane, R. Sasikala, B. Vishwanadh, V. Sudarsan, S Mahamuni, international journal of hydrogen energy 38 (2013) 15012.

[23] N. K. Morozova, A. A. Kanakhin, I. N. Miroshnikova, and V. G. Galstyan, Semiconductors 47(2013)1018.

[24] F. Ballipinar, A. C. Rastogi, Journal of applied physics 121 (2017) 035302.

[25] L. Lutterotti, Nucl. Inst. Methods, Phys. Res. B. 268 (2010)334.

[26] J. Rodríguez-Carvajal, Phys. B (Amsterdam, Neth.) 192 (1993) 55.

[27] J. Perdew, J.A. Chevary, S.H. Vosko, K.A. Jackson, M.R. Pederson, D.J. Singh, C. Fiolhais, Phys. Rev. B Condens. Matter 46 (1992) 6671.

[28] J.P. Perdew, Y. Wang, Phys. Rev. B 45 (1992)13244.

[29] J.P. Perdew, K. Burke, M. Ernzerhof, Phys.Rev. Lett 77 (1996) 3865.

[30] Z.K. Heiba, Cryst. Res. Technol. 38(6) (2003)488.

[31] Z.K. Heiba, Powder Diffraction 17 (3) (2002) 191.

[32] N. Susha, K. Nandakumar, S S. Nair, RSC Adv. 8 (2018)11330.

[33] S.B. Qadri, E.F. Skelton, D. Hsu, A.D. Dinsmore, J. Yang, H.F. Gray, Phys. Rev. B 44 (1999)153.

[34] S. Ummartyotin, N. Bunnak, J. Juntaro, M. Sain, and H. Manuspiya, Solid State Sci., 14(3) (2012)299.

[35] K. I. Hadjiivanov, D. A. Panayotov, M. Y. Mihaylov, E. Z. Ivanova, K. K. Chakarova, S. M. Andonova, N. L. Drenchev, Chem. Rev. 2020, https://doi.org/10.1021/acs.chemrev.0c00487.

[36] X. Li, D. L. Young, H. Moutinho, Y. Yan, C. Narayanswamy, T. A. Gessert, T. J. Coutts, Electrochem. Solid State 4 (2001) C43.

[37] ZK Heiba, AA Albassam, MB Mohamed, Applied Physics A 126 (2020) 479.

[38] C. Persson, C. Platzer-Björkman, J. Malmström, T. Törndahl, M. Edoff, Phys. Rev. Lett. 97 (2006) 146403.

[39] M. Ishikawa, T. Nakayama, Phys. Status Solidi C 10 (2013) 1385.

[40] X.S. Zhao, J. Schroeder, P.D. Persans, T.G. Bilodeau, Phys. Rev. B 43 (1991)12580.

[41] N. Chestnoy, T.D. Harris, R. Hull, L.E. Brus, J. Phys. Chem. 90 (1986) 3393.

[43] J. Chrysochoos, J. Phys. Chem. 96 (1992) 2868.

[44] B. Zhou, Z. Liu, H. Wang, Y. Yang, W. Su, Catal. Lett. 132 (2009) 75.

[45] C. Wang, H.M. Wang, Z.Y. Fang, J. Alloys Compd. 486 (2009) 702.

[46] S. K. Mishra, R. K. Srivastava, S.G. Prakash, R. S. Yadav, A.C. Panday, Electronic Materials Letters,7(1) (2011)31.

[47] I. López, I. Gómez, Physica B Condensed Matter 453(2014)81.

[48] S. Muruganandam, G. Anbalagan, G. Murugadoss, Indian J Phys, 89(2015)835.

[49] K. Kaur, N K Verma, Journal of Superconductivity and Novel Magnetism, 28(11) (2015) 3317.

[50] Pradyumna Elavarthi, Astakala Anil Kumar, G. Murali, D. Amaranatha Reddy, K.R. Gunasekhar, Journal of Alloys and Compounds 656 (2016)510.

[51] S. V. Kahane, R. Sasikala, B. Vishwanadh, V. Sudarsan, S, Mahamuni, international journal o f hydrogen energy 38 (2013) 15012.

[52] L. Huang, J.Yang, X. Wang, J. Han, H. Han, C. Li. Phys Chem Chem Phys 15 (2013)553.

[53] ZK Heiba, MB Mohamed, AM Wahba, J Mater Sci: Mater Electron. 31 (17) (2020) 14645.

[54] S.Z. Karazhanov, P. Ravindran, A. Kjekshus, H. Fjellvag, B.G. Svensson, Phys. Rev. B 75 (2007) 155104

[55] M. Junaid Iqbal Khan et al., J. Alloys Compd. 695 (2016)3605.

[56] M. A. Habeeb, Mater. Focus 5 (2016) 550.

[57] M. J. I. Khan, Z. Kanwal, J. Liuy, A. Ijazz, N. Usmani, International Journal of Modern Physics B, 33(31) (2019) 1950381.

Tables

Table1. Lattice parameter, a (Å), average crystallite size nm, and phase percentage for CdS_{1-x} samples.

x	CdS							
	Cubic			Hexa P 6_3 m c				
	a	size	%	*a*	*c*	size	z(S/O)	%
0.0	5.875(4)	6	55	4.131 (3)	6.787(4)	5	0.3781	45
0.03	5.837	5	55	4.125	6.780	5	0.3741	45
0.05	5.828	4	57	4.120	6.778	5	0.3698	43
0.10	5.831	5	54	4.123	6.775	6	0.3679	46

Table 2. PL peak positions for CdS_{1-x} samples, V=violet, B=blue, G=green and O=Orange.

	CdS_{1-x}	
x	PL peaks positions (nm)	
	excitation wavelength 350 nm	excitation wavelength 375 nm
0	409 (V), 442(B), 509(G)	420 (B), 500(G), 565(G)
0.03	407 (V), 447(B), 497(G), 534 (G), 624 (O)	430 (B), 510(G), 622(O)
0.05	427(B), 511 (G), 568 (G), 614(O)	407(V),472 (B)
0.1	411 (V), 438(B), 480(B)	429(B), 443(B), 547(G), 618(O)

Figures

Figure 1

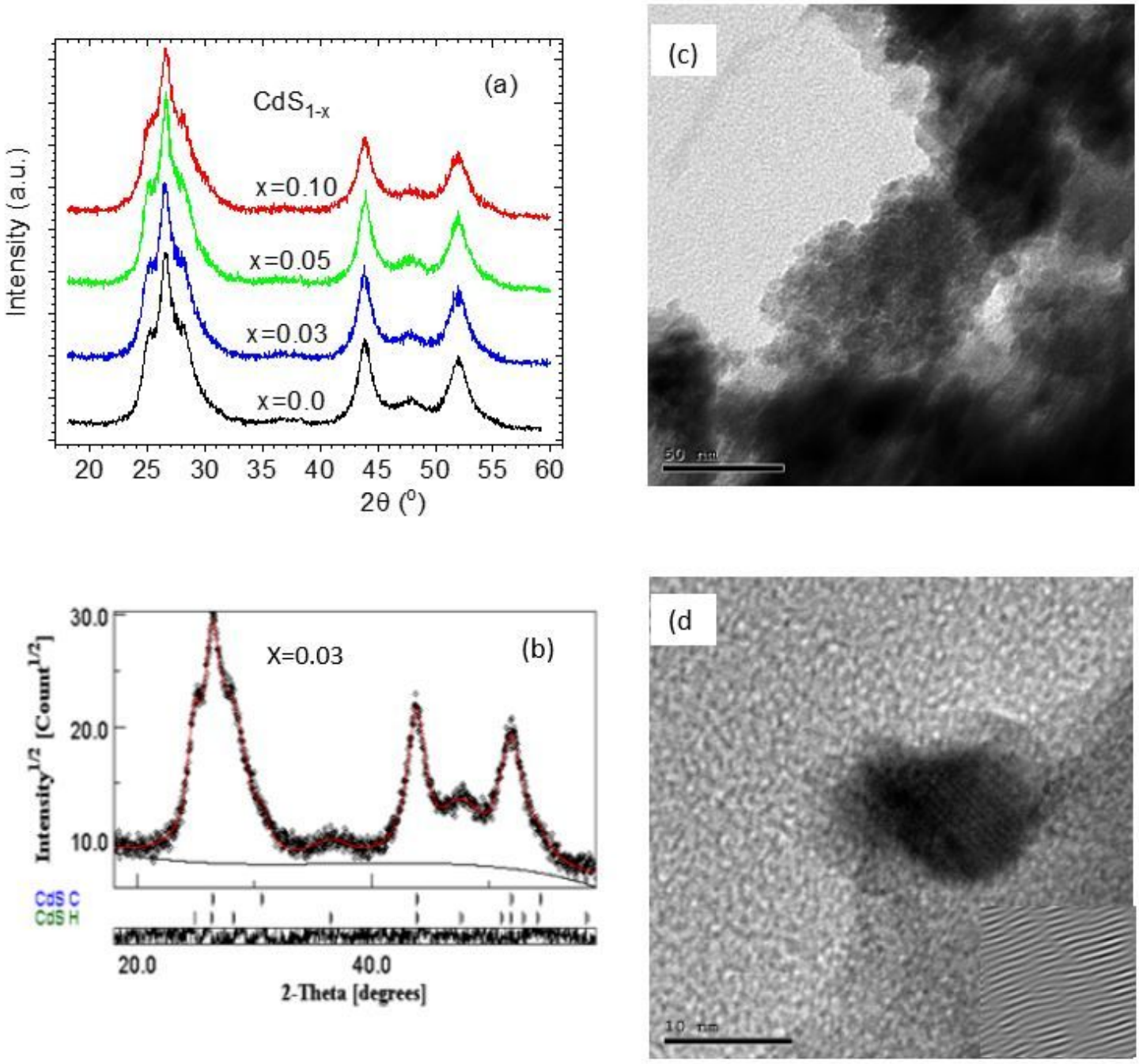

Figure 2

(a) XRD patterns, (b) Rietveld refinement for CdS0.97 samples, and (c, d) TEM images with different magnifications for nano CdS0.9.

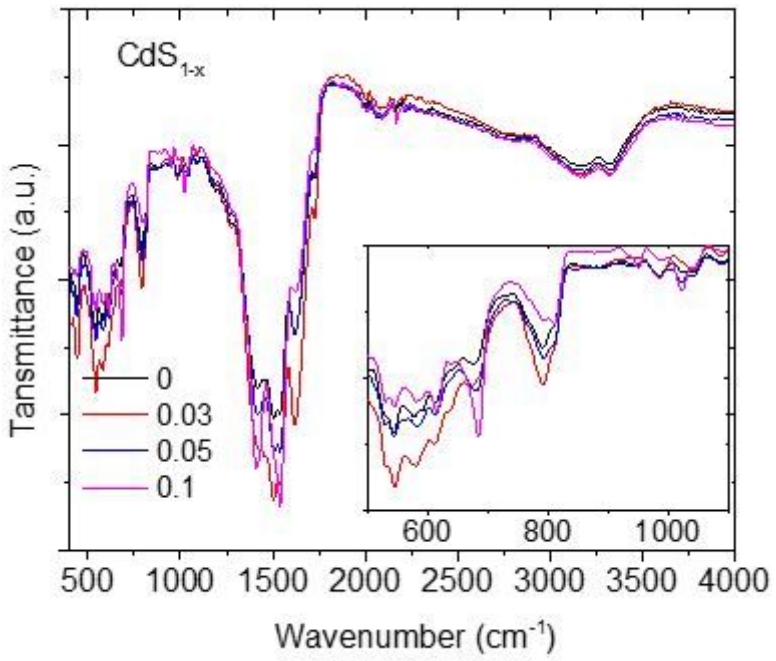

Figure 3

FTIR for CdS1-x nano system.

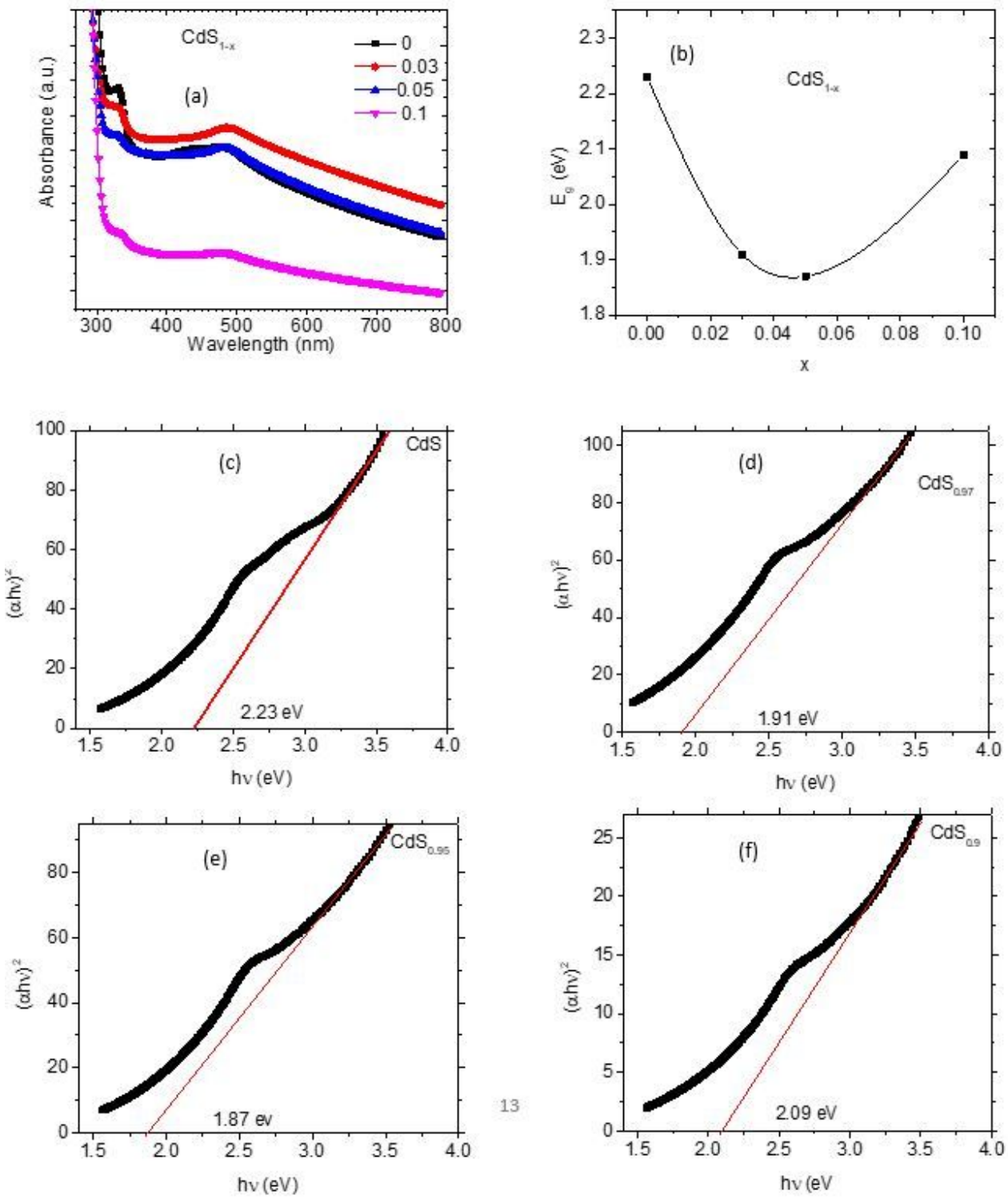

13

Figure 4

(a)UV-vis absorption spectra, (b) composition dependent of energy gap and (c, d, e, f) plot of (ahυ)2 vs hυ for CdS1-x samples.

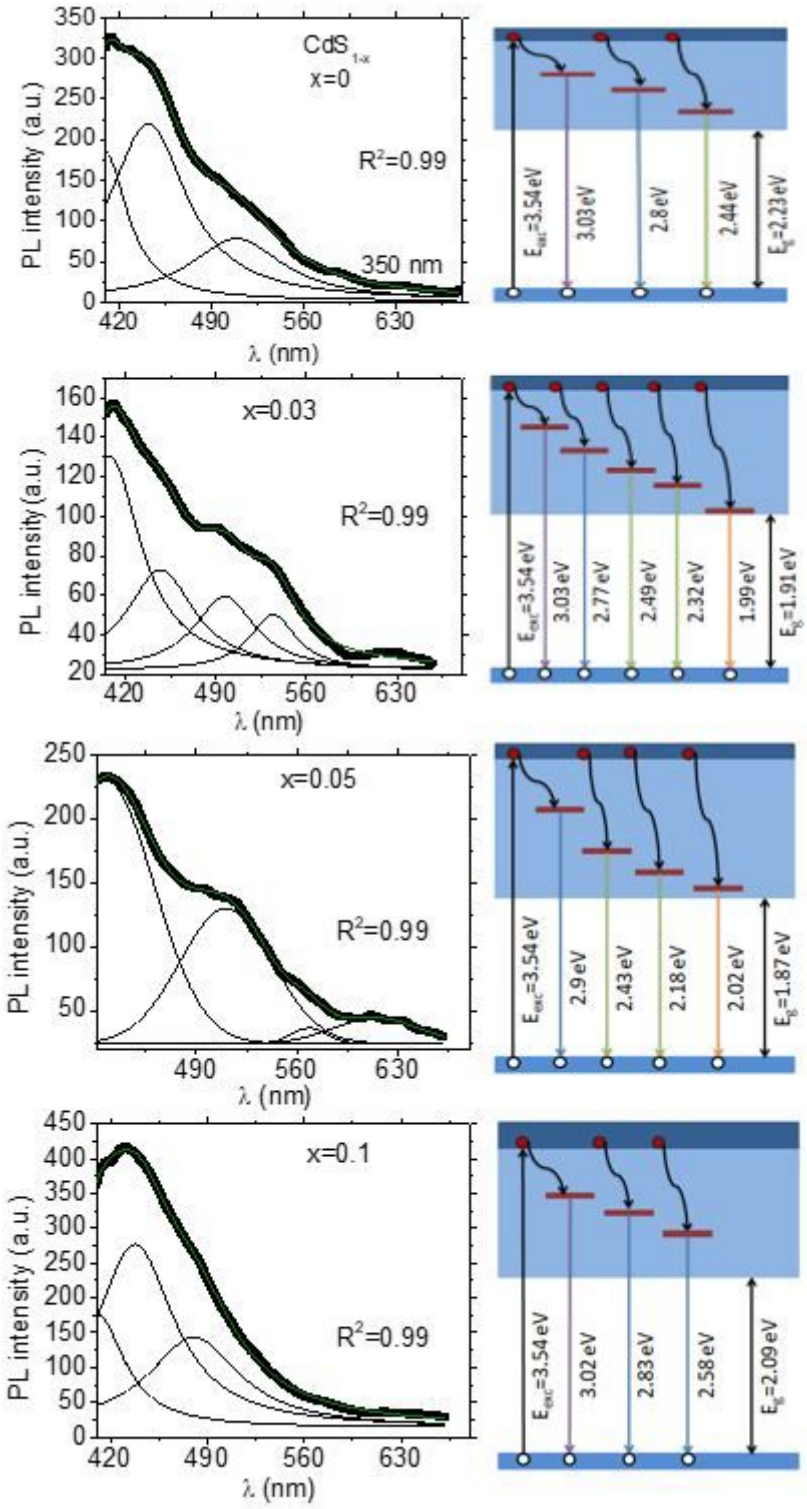

Figure 5

Gaussian fitting of photoluminescence measurements and the corresponding schematic of various possible transitions for CdS1-x system under 350 nm excitation wavelength, balls with red and white colors represent the electron and the hole, respectively.

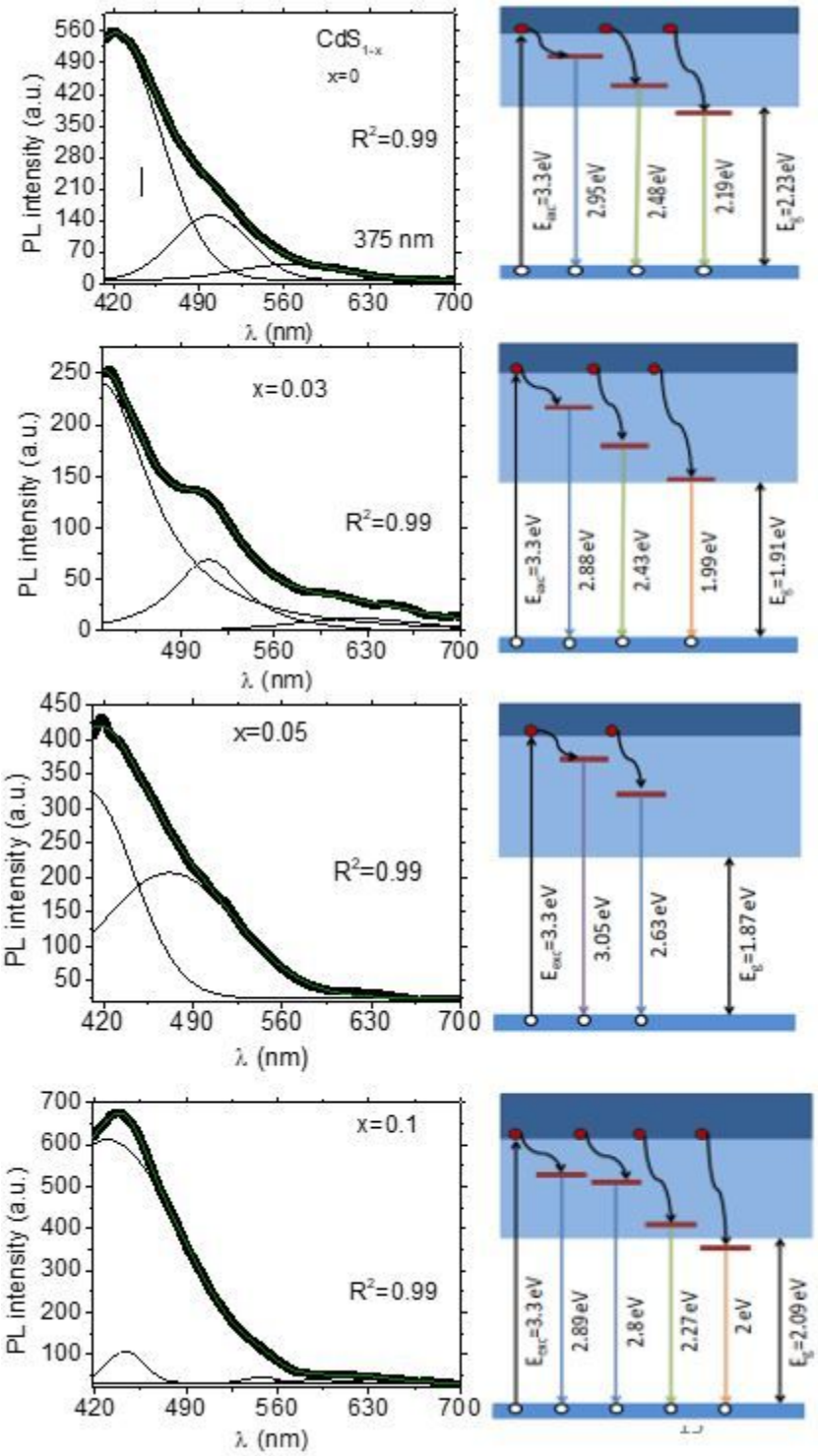

Figure 6

Gaussian fitting of photoluminescence measurements and the corresponding schematic of various possible transitions for CdS1-x system under 375 nm excitation wavelength, balls with red and white colors represent the electron and the hole, respectively.

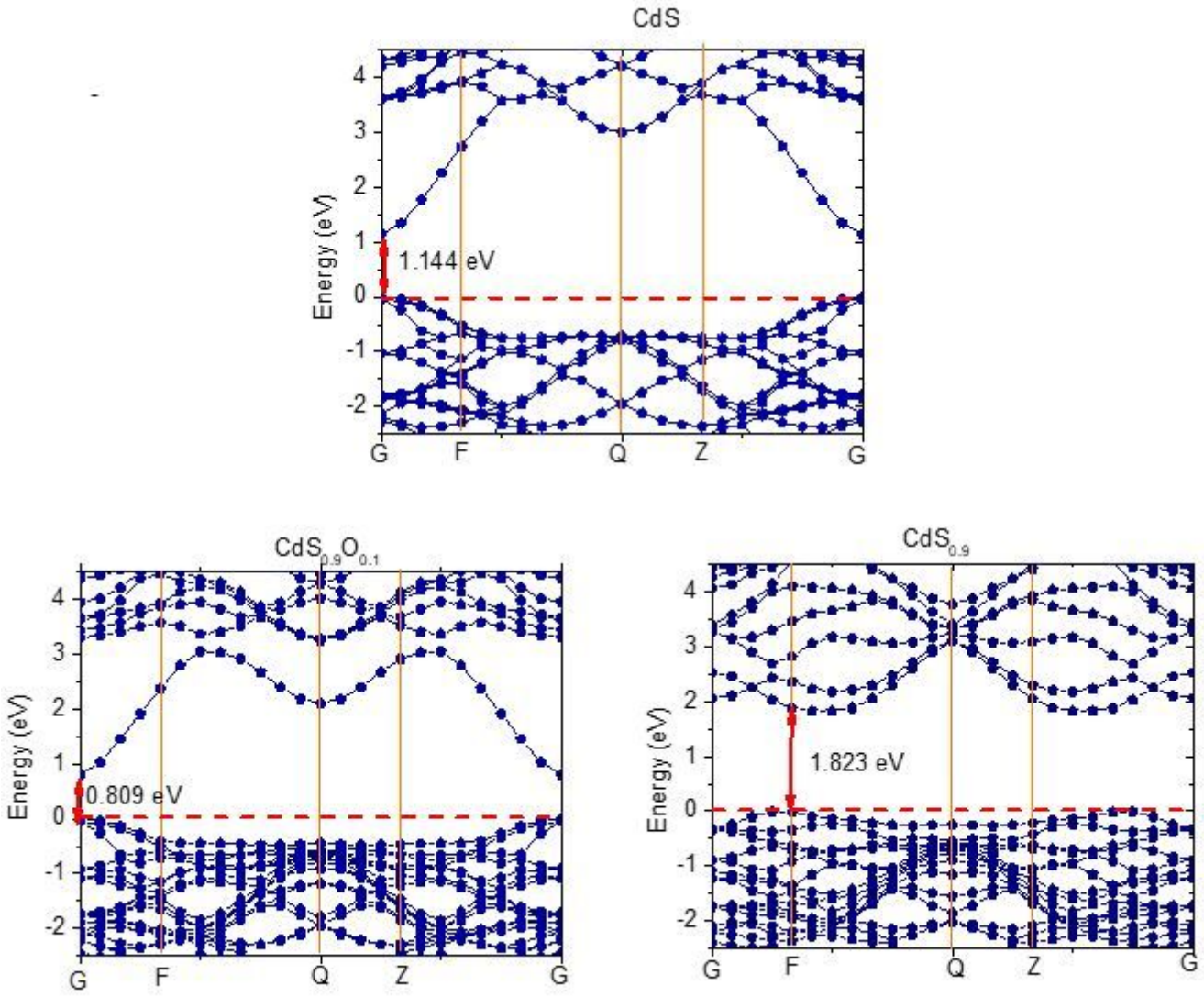

Figure 7

The electronic band structure for CdS, CdS0.9O0.1 and CdS0.9 samples.

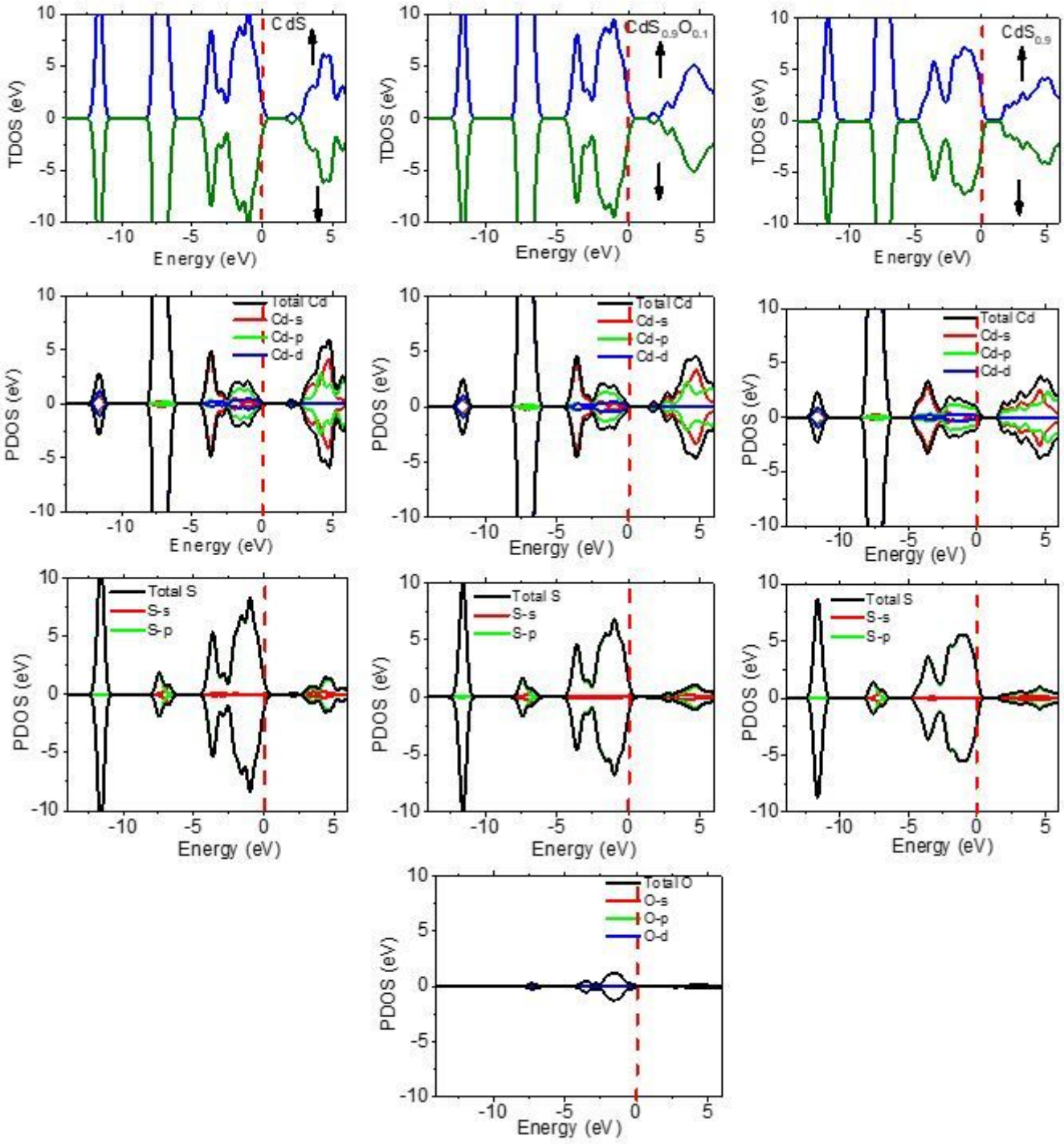

Figure 8

Total (DOS) and partial density of states (PDOS) for CdS, CdS0.9O0.1 and CdS0.9 samples.

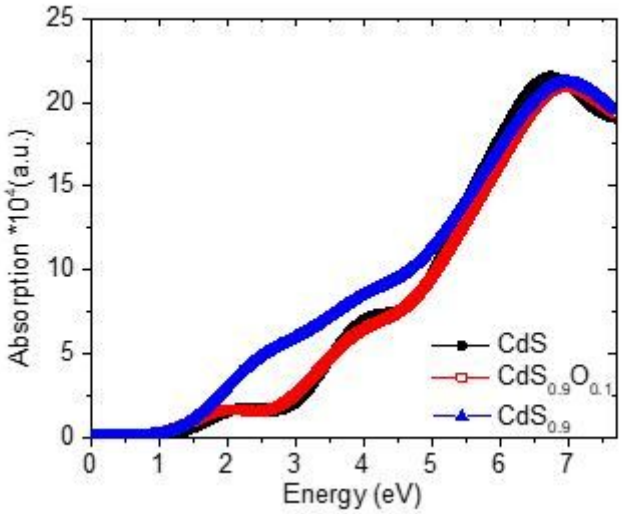

Figure 9

The optical absorption for CdS, CdS0.9O0.1 and CdS0.9 samples.

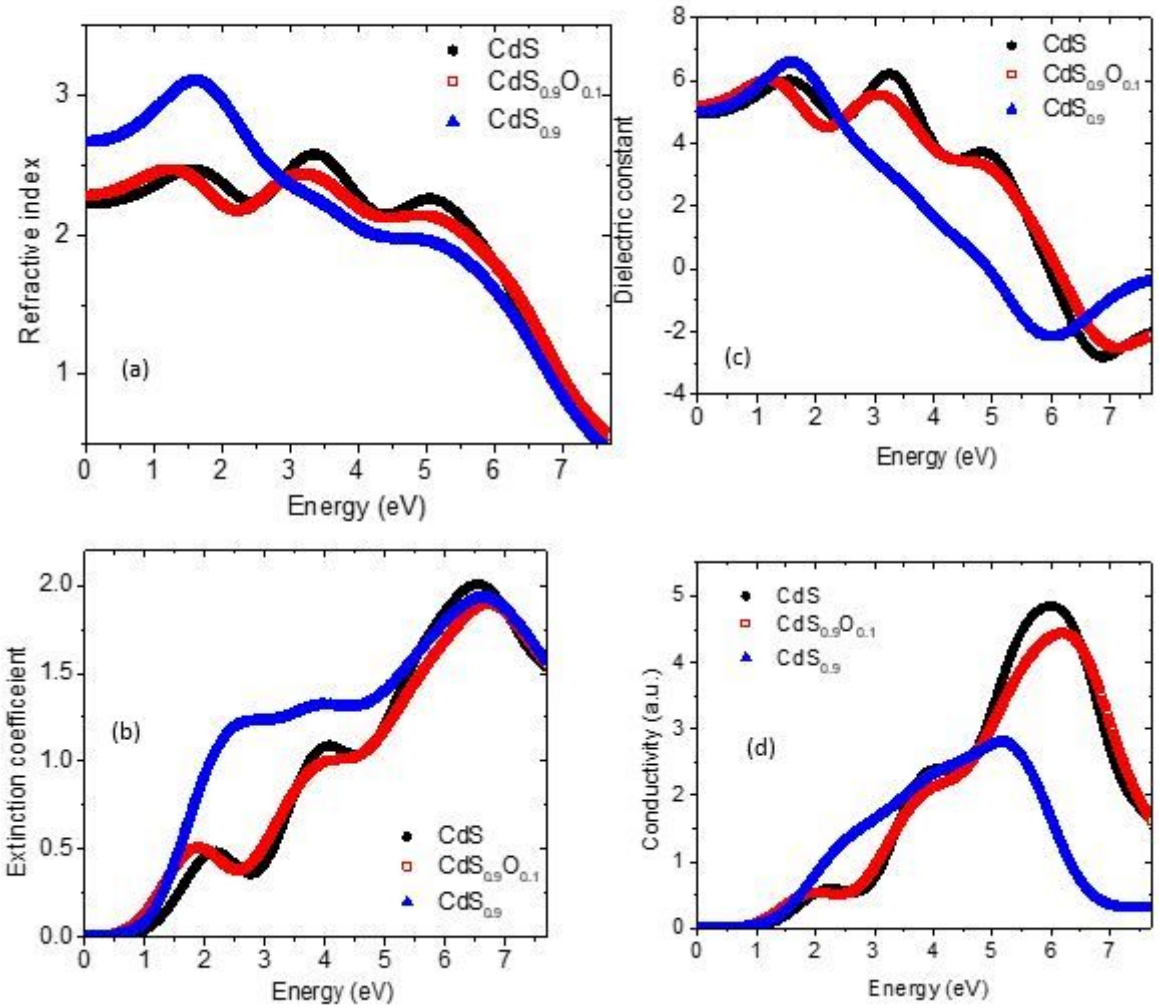

Figure 10

The optical functions: (a) refractive index, (b) extinction, (c) dielectric constant and (d) optical conductivity for CdS, CdS0.9O0.1 and CdS0.9 samples.